Ionization relaxation in a plasma produced by a pulsed inert-gas discharge

A. A. Kudryavtsev and V. N. Skrebov

A. A. Zhdanov State University, Leningrad

A model is developed for the initial stage of ionization relaxation in a pulsed inert-gas discharge plasma at moderate pressures for E/n_1 values corresponding to ionization levels $n_e^0/n_1^0 \gg 10^{-4}$. It is shown that the electron density increases explosively in time due to accumulation of atoms in the lowest excited states. An approximate analytic solution is found for describing the behavior of the time and spatial increase in n_e as a function of the specific conditions. The proposed model is verified experimentally.

PACS numbers: 52.25.Lp, 51.50. + v, 52.80.Dy

The study of ionization relaxation in a plasma when the external electric field suddenly increases is of great importance in many areas of gas discharge physics and its applications. Interest in ionization relaxation in inert gas discharges has been stimulated recently by the rapid development of excimer lasers excited by pulsed electrical discharges (see, e.g., Ref. 1). In the present work we study ionization relaxation in an inert gas plasma at moderate pressures when the electric field strength increases discontinuously and the ratio E/n_1 and degree of ionization n_e/n_1 vary over a wide range.

In this paper we consider the initial stage of ionization relaxation when the ionization n_e/n_1 increases from the initial value $n_{e0}/n_1 = 10^{-8}$–10^{-7} to 10^{-5}–10^{-4}. We are mainly interested in analyzing the buildup of n_e and the behavior of the spatial distribution of n_e during the relaxation process. We report experimental data on ionization relaxation in the range $8 < E/n_1 \lesssim 30$–40 Td.

THEORY

In general, the increase in the electron density n_e in a plasma when the electric field E increases abruptly is described by a nonlinear system of kinetic balance equations which cannot be solved analytically because of the usual difficulties.

In this section we derive an approximate dynamic model of ionization that is based on theoretical results on various aspects of ionization relaxation in Refs. 2–9.

1. When E/n_1 increases discontinuously, the relaxation time for the electron energy distribution function for $E/n_1 \gtrsim 3$ Td is much less than the characteristic ionization growth times ($t_r < 1$ μs).[2,3] Therefore, the kinetic electron coefficients do not depend on time explicitly but are functions of the parameters E/n_1, n_e/n_1, and the nature of the ionized atoms. In what follows, we assume that these parameters are known either from published experimental data or from numerical solution of the Boltzmann kinetic equation.[5,6]

2. If we use k to label the excited states (with k = 2 corresponding to the first excited state), the populations of the excited states with k > 2 are almost always quasistationary. However, quasistationarity may be violated for the lower metastable or resonance levels when n_e is small and radiation capture predominates. The balance equation for these levels must therefore be formulated in differential form after first combining the states into a single effective level characterized by an average energy and total statistical weight.

3. Because of the importance of the transition $k \rightleftharpoons k \pm 1$ in the collisional transition kinetics between excited states, it is helpful when describing the atomic distribution over the excited states with k > 2 to use the machinery of the modified diffusion approximation (MDA) theory,[4,5] which gives the quasistationary populations in terms of n_e and n_2.

4. Since for E/n_1 in the range of interest the ionization n_e^0/n_1^0 is much greater than 10^{-4}, we may neglect radiative processes and three-body collisions.

5. The data in Refs. 7, 8 on the rate constants for formation of molecular ions and excimer molecules show that we may assume that these processes have little influence on the ionization growth rate when an electric field is suddenly applied to a weakly stabilized inert gas at moderate pressures [$n_1 < (5$–$7) \cdot 10^{17}$ cm^{-3}]. It can be shown using the arguments in Ref. 4 that under these conditions the associative ionization channel is of minor importance compared with the stepwise ionization channel.

Using the above remarks, we can describe the ionization relaxation using the following system of equations:

$$\frac{\partial n_e}{\partial t} = n_1 n_e \beta_{1e} + n_2 n_e \beta_{2e} + n_2 n_e \beta_{st} - \nabla \Gamma_e, \tag{1}$$

$$\frac{\partial n_2}{\partial t} = n_1 n_e k_{12} - n_2 n_e k_{21} - n_2 n_e \beta_{2e} - n_2 n_e \beta_{st} - n_2 A_{21} \theta_{21} - \nabla \Gamma_2. \tag{2}$$

Here n_1, n_2, and n_e are the atomic densities in the ground and first excited states and the electron density, respectively; k_{12}, k_{21} are the rate constants for the collisional transitions $1 \rightleftharpoons 2$; β_{1e} and β_{2e} are the rate coefficients for
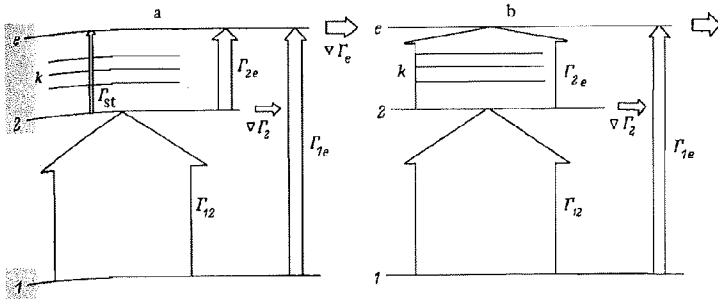
FIG. 1. Diagram showing the relative sizes of the electron fluxes in terms of the atomic energy levels for the slow (a) and fast (b) stages. The width of the arrows indicates the magnitude of the electron flux. The horizontal arrows give the diffusion fluxes of electrons and excited atoms reaching the walls of the discharge tube.

direct ionization from the ground state to the first excited level; β_{st} is a generalized coefficient for stepwise ionization from the quasistationary levels (k > 2); A_{21} is the spontaneous transition probability $2 \to 1$; θ_{21} is the capture factor for resonance radiation, calculated using the Biberman–Holstein equations[4]; $\nabla \Gamma_e$ and $\nabla \Gamma_2$ are the diffusion fluxes of the electrons and excited atoms, and are given approximately by $\nabla \Gamma_k \simeq n_k \nu_{Dk}$ [for a cylindrical geometry, $\nu_{Dk} \simeq (2.4)^2 D_k / R^2$].

It can be shown using the MDA theory[4] that

$$n_2 n_e \beta_{st} = n_2 n_e \beta \frac{2 \overline{\Lambda}}{3 \sqrt{\pi} g_2} \frac{1}{\Pi_2} \left(\frac{Ry}{T_e} \right)^3 \frac{e^{-E_2/T_e}}{\chi \left(\frac{E_k}{T_e} \right)}, \qquad (3)$$

where

$$\Pi_2 = \exp(0.2 E_{2l}^4 / E_k^4),$$

$$E_k = (n_e / 4.5 \cdot 10^{13})^{1/4} T_e^{-1/4} \quad (n_e - \text{in cm}^{-3}, \ T_e - \text{in eV}),$$

$$\overline{\Lambda} \simeq 0.2, \quad Ry = 13.6 \ \text{eV}, \quad \chi(x) = \frac{4}{3 \sqrt{\pi}} \int_0^x e^{-t} t^{1/2} dt,$$

$$\beta = \frac{4 \sqrt{2\pi} \, e^4}{\sqrt{m} \, Ry^{3/2}} \simeq 1.7 \cdot 10^{-7} \ \text{cm}^3/\text{s}. \qquad (4)$$

To facilitate comparison, we have retained the notation used in Ref. 4.

The nonlinear system (1)–(2) can be solved numerically if the coefficients and initial conditions are specified. Using the rate constants given in Refs. 5–8 for the various processes, we can make a series of simplifications making it possible to solve (1)–(2) analytically for E/n_1 and n_e/n_1 in the range of interest.

Since $\beta_{2e} \simeq 10^{-8}$–$10^{-7}$ cm^3/s [Refs. 5, 8], we see from (3) and (4) that the ratio β_{2e}/β_{st} of the coefficients for direct and stepwise ionization from the first excited level depends on n_e and on the electron temperature T_e. For $n_e < 5 \cdot 10^{13}$ cm^{-3} and $T_e \gtrsim 1$ eV, the stepwise ionization channel from levels with k > 2 is unimportant ($\beta_{st} \ll \beta_{2e}$) because most of the radiation escapes.
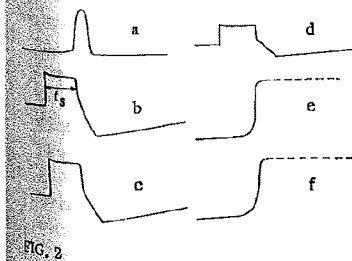

FIG. 2

Estimates using the equations in Ref. 4 show that under typical conditions (R $\gtrsim$ 1 cm, $n_1 \gtrsim 10^{16}$ cm^{-3}), the radiation capture factor is $\theta_{21} \simeq 10^{-3}$–$10^{-4}$. Therefore, the effective radiative lifetime of level 2 is long and the level may be regarded as quasimetastable.

Under these same conditions, the characteristic excited atom diffusion times are $\tau_{D2} \simeq 10^{-3}$–10^{-2} s, so that we may neglect $\nabla \Gamma_2$ compared with $n_2 n_e \beta_{2e}$ in (2).

The above arguments show that the three-level approximation can be used to describe ionization buildup under our assumptions. In dimensionless variables, the equations for the ionization kinetics take the form

$$\partial N / \partial \tau = bNM + cN - dN, \qquad (5)$$

$$\partial M / \partial \tau = N - bNM,$$

$$M = n_2/n_{e0}, \quad N = n_e/n_{e0}, \quad \tau = t n_1 k_{12}, \quad M|_{\tau=0} = M_0, \quad N|_{\tau=0} = 1,$$
$$b = n_{e0} \beta_{2e} / n_1 k_{12}, \quad c = \beta_{1e}/k_{12}, \quad d = \nu_{Du}/n_1 k_{12}. \qquad (6)$$

Equations (5)–(6) easily yield the following relation between N and M:

$$N = 1 + M_0 - M + \frac{(1 + c - d)}{b} \ln \left[\frac{(1 - bM_0)}{(1 - bM)} \right] \qquad (7)$$

so that the solution reduces to a quadrature.

Using the rate constant data in Ref. 5, we find that b $\ll$ 1 and c $\ll$ 1 in all cases of practical interest (E/n_1 < 300 Td, $n_e/n_1 < 10^{-5}$). In a steady-state plasma, we usually have $M_0 \lesssim 1$ [Ref. 9].

Using the smallness of b and c, we find from (5)–(7) that $dN/dM \simeq c - d + bM_0 \ll 1$ in the initial stage, i.e., the number of atoms in the first excited states increases rapidly for a relatively slow change in the electron density. The rate of ionization then increases with time and rises most steeply for M > c/b. For nearly stationary n_2 values (M = 1/b), so that n_2 is changing slowly, there is an explosive increase in n_e. The subsequent increase in n_e then reaches its maximum value, equal to the rate of excitation $dN/d\tau = N(1 + c - d)$, which is several orders of magnitude greater than the ionization rate during the initial stage.

The behavior of the increase in n_e with time thus enables us to arbitrarily divide the ionization process into two stages, which we will call the slow and fast growth stages. Figure 1 illustrates the relationships between the main electron currents in terms of the atomic energy levels during the slow and the fast stages.

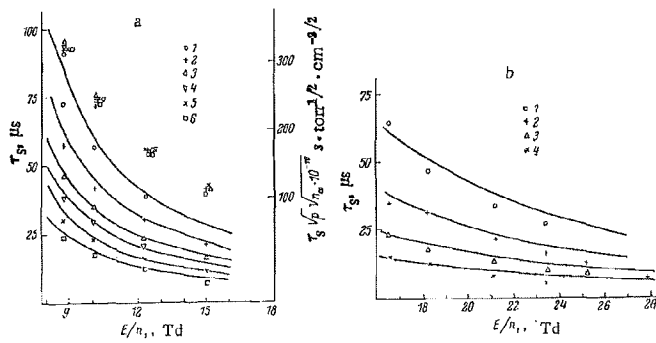Since n_e rises at an ever increasing rate (which is several orders of magnitude larger than the initial rate)

A. A. Kudryavtsev and V. N. Skrebov

FIG. 3. Duration τ_s for a discharge in argon. $p = 11.4$ (a) and 3.7 torr (b). a: 1) $n_{e0} = 1.6 \cdot 10^{10}$ cm^{-3}; 2) $2.7 \cdot 10^{10}$; 3) $4.5 \cdot 10^{10}$; 4) $6.4 \cdot 10^{10}$; 5) 10^{11}; 6) $1.6 \cdot 10^{11}$; b: 1) $9.7 \cdot 10^9$; 2) $3 \cdot 10^{10}$; 3) $6.8 \cdot 10^{10}$; 4) $1.6 \cdot 10^{11}$.

once steady conditions have been reached during the fast stage, ionization builds up explosively when the external field is constant (the kinetics of gas-phase reactions are classified in Ref. 10).

We can solve Eqs. (5)–(7) analytically and thus analyze in more detail the behavior of $n_e(t)$ and $n_2(t)$ as ionization develops.

Since $bM < 1$ during the slow stage, if we keep only the linear terms in bM in (7) we find from (5)–(7) that

$$N = bM^2/2 + (c - d) M + 1 - bM_0^2/2 - (c - d) M_0, \tag{8}$$

$$\tau = \frac{2}{b \sqrt{|A|}}$$

$$\times \begin{cases} \frac{1}{2} \ln \left[\frac{(bM + c - d - b\sqrt{|A|})(bM_0 + c - d + b\sqrt{|A|})}{(bM + c - d + b\sqrt{|A|})(bM_0 + c - d - b\sqrt{|A|})} \right], & A < 0, \quad (9a) \\ \operatorname{arctg}\left[\frac{bM + c - d}{b\sqrt{|A|}}\right] - \operatorname{arctg}\left[\frac{bM_0 + c - d}{b\sqrt{|A|}}\right], & A > 0, \quad (9b) \end{cases}$$

where A is given by

$$A = (2/b) - [M_0 + (c - d)/b]^2 \tag{10}$$

and describes the relative contribution from the various processes in (5) for small times.

The conditions for n_e to increase with time are that ionization should always develop eventually if $A > 0$; if $A \le 0$, the condition is that $bM_0 + c > d$.

It can be shown using (6), (7) that the curve $M(\tau)$ has an inflection point at $M_1 = N_1 - (c - d)/b \simeq 0.8/b$, after which M changes slowly. Since M_1 differs from the stationary value by 20% and the various rate constants are only known to within a factor of two,[5] may assume without any loss of accuracy that at subsequent times the ionization has become stationary:

$$M = \frac{1}{b}, \quad \tau = \frac{1}{(1 + c - d)} \ln \frac{N}{N_1}. \tag{11}$$

The rate constants for the elementary processes are known accurately enough to permit Eqs. (9) above to be used to describe the time changes in n_e and n_2 as far as the inflection point $M = M_1$.

Equations (9), (11) derived above readily yield expressions for the characteristic times of the slow and fast stages. Since we have $bM + c - d \gg b\sqrt{|A|}$ prior to the start of the abrupt rise in n_e, the duration τ_s of the slow stage can be found with sufficient accuracy from (9) by setting the first quotient in the logarithm in (9a) equal to one

and taking the first arctangent in (9b) equal to $\pi/2$. Equation (11) shows that the characteristic time for the fast stage is $\tau \approx \ln(N/N_1) \ll \tau_s$. We see by inspecting the form of the above solutions that n_e builds up explosively with time.

It should be emphasized that the reason for this behavior in $n_e(t)$ is quite universal and can be traced to the fact that we almost always have $\beta_{1e} \ll k_{12}$.

The explosive increase in $n_e(t)$ is most apparent when $A > 0$, which corresponds to early times and small direct ionization. In this case, n_e does not increase more than tenfold prior to the onset of explosive growth [$M > \sqrt{(2/b)}$].

These expressions can be used to determine the limits of applicability of the two simplest ionization models which are often used in practical calculations. These are the direct ionization model, in which the ionization is determined by the appropriate rate constant or by the first Townsend coefficient, and the "instantaneous ionization" model, in which the ionization rate is taken equal to the rate of excitation. Equations (8)–(11) imply that direct ionization predominates only for times $\tau < \tau_1$ ($M = \sqrt{2/b}$) after the field is applied, and that the "instantaneous ionization" approximation does not become valid until times $t \approx \tau_s$ after the field was first switched on.

EXPERIMENTAL RESULTS

We studied ionization relaxation in He, Ne, Ar, and Kr for initial gas densities $n_1 = (0.5-5) \cdot 10^{17}$ cm^{-3} by applying an additional electric field to the preionized gas. The discharge occurred inside a cylindrical tube of diameter $2R = 2.5$ cm and the distance between the electrodes was $L = 52$ cm. The gas was preionized by applying a dc current $i_p = 0.5-20$ mA. The parameters of the positive plasma column were calculated using the theory developed in Ref. 9 from the experimentally recorded current density and E_0/n_1 values. The initial density n_{e0} on the axis varied in the range $5 \cdot 10^9 - 4 \cdot 10^{11}$ cm^{-3}.

A voltage pulse with rise time $(1-2) \cdot 10^{-7}$ s of positive polarity with respect to the cathode was applied to the tube using a specially designed electrical circuit. The electric field was measured using several detectors soldered into the tube along its axis. The total voltage across the tube and the voltage between the probes were recorded by a capacitative divider ($C_1 = 2$ pF and $C_2 = 100$ pF) capable of transmitting rectangular pulses with rise time $\sim 10^{-7}$ s without appreciable distortion. The discharge current was recorded using a zero-inductance

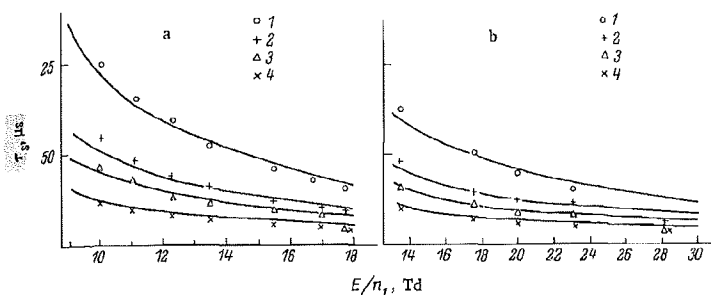A. A. Kudryavtsev and V. N. Skrebov

32

FIG. 4. Curves for τ_s vs. E/n_1 for a discharge in krypton; $p = 10.5$ (a) and 6 torr (b). a: 1) $n_{e0} = 4 \cdot 10^{10}$ cm^{-3}; 2) 10^{11}; 3) $1.5 \cdot 10^{11}$; 4) $3.3 \cdot 10^{11}$; b: 1) $3.5 \cdot 10^{10}$; 2) $9.5 \cdot 10^{10}$; 3) $1.6 \cdot 10^{10}$; 4) $3.2 \cdot 10^{11}$.

resistor connected in series with the cathode-to-ground section of the tube. The local dependences $n_e(t)$ were recorded by observing the plasma emission intensity, which is proportional to n_e^p ($p \geq 1$). The density of the neutral gas was monitored using the interferometric technique described in Ref. 11 and a dual-trace oscilloscope was used for all the measurements. Special experiments were conducted to verify the unimportance of such factors as the proximity of the shields and grounded objects or the shape and composition of the electrodes (we had $pL > 200$ cm·torr [Ref. 12]), which do cause appreciable effects during breakdown of a cold gas.[12,13] We were also able to reproduce the experimental conditions with high accuracy. We measured E and the plasma emission intensity at different distances along the tube axis in order to find how the parameters of the gas discharge plasma vary along the tube and ascertain the importance of various mechanisms involved in discharge formation after an abrupt increase in the field strength.

Figure 2 shows some typical measured curves. The oscilloscope traces of the current (a), tube voltage (b), voltage differences between the probes (c, d), and the emission from different regions along the length of the discharge (e, f) show that after a high-voltage pulse is suddenly applied, the discharge current rises very slowly for times $t < \tau_s$ and the tube voltage remains almost constant. This is followed by a sudden rise in the current, accompanied by a voltage drop across the tube. We also see that the field increases almost simultaneously (to within 10^{-7} s) over the entire length of the positive column and then remains constant for $t < \tau_S$. The plasma emission intensity from different regions along the length of the tube also starts to increase almost simultaneously and repeats the current trace.

Our measurements revealed that for $t < \tau_S$, n_e/n_1 increases by less than a factor of 10^2, i.e., we have $n_e/n_1 < 10^{-5}$ at the end of the slow stage.

A similar delay in the current increase has been noted by many other workers when an electric field is suddenly applied (see e.g., Ref. 12). This lag might be caused by the small velocity of the ionization wave down the tube from the high-voltage electrode to the grounded electrode,[13,14] or by onset of instability in the uniform quasistationary discharge when the field is applied [possibly caused by processes near the electrodes; cf. Ref. 15]. Taken together the above findings show that in any case, neither propagation of an ionization wave nor processes at the electrodes determine the duration τ_S of the slow stage.
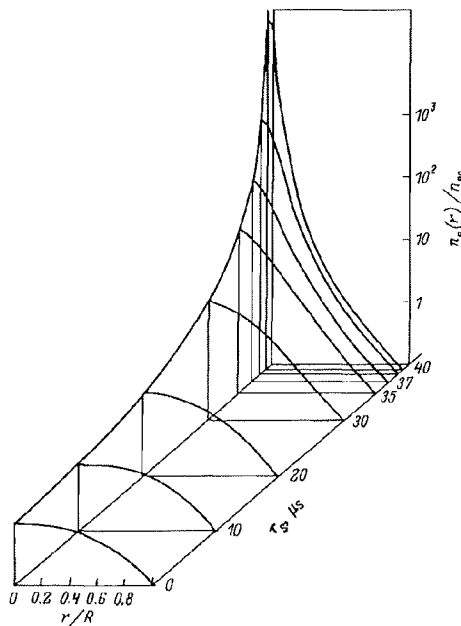
The lag in rapid current buildup has often[16,17] been

FIG. 5. Radial distribution $n_e(r)$ as a function of time for A > 0 in an argon discharge. $p = 11.4$ torr, $n_{e0} = 10^{10}$ cm^{-3}, $\tau_s = 39$ μs.

attributed to the finite time required for growth of thermal-ionization instability. Interferometric measurements show that for $t < \tau_S$ the gas density does not drop by more than 1%. Estimates using the equations in Ref. 16 reveal that for such small changes in n_1, the growth time for thermal-ionization instability is much larger than τ_S.

Thus, under our conditions the slow increase in n_e during the initial stage is due to the combined effects of kinetic processes occurring in the bulk of the discharge for constant E/n_1, quasistationary electron energy distribution functions, and n_e/n_1 values $< 10^{-5}$.

We now compare the experimental results for Ar and Kr with the theory developed above.

The points in Figs. 3, 4 give the experimental values as a function of the specific conditions (n_1, n_{e0}, E/n_1). Since in our experiments we had A > 0 [cf. (10)], Eq. (9b) implies that the duration of the slow stage is given by

$$\tau_s = \sqrt{\frac{2}{b}} \frac{1}{\sqrt{1 - \frac{b}{2}\left(M_0 + \frac{c-d}{b}\right)^2}} \arctan\left[\frac{\sqrt{b/2}\,[M_0 + (c-d)/b]}{\sqrt{1 - \frac{b}{2}\left(M_0 + \frac{c-d}{b}\right)^2}}\right].$$

$$(12)$$

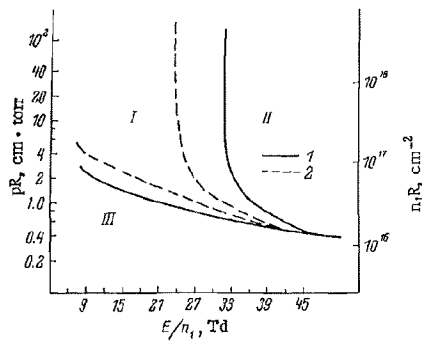A. A. Kudryavtsev and V. N. Skrebov   33

FIG. 6. The behavior of n_e in the bulk of an argon discharge. 1) $n_{e0}/n_1 = 10^{-8}$; 2) 10^{-7}. Stepwise ionization predominates in region I, direct ionization processes predominate in region II, and n_e does not increase in region III.

The solid curves in Figs. 3, 4 give τ_s calculated from (12) using values for k_{12}, β_{1e}, and β_{2e} from numerical calculations in Ref. 5.

Equation (12) shows that for small E/n_1, when $A \simeq 2/b$, we have $\tau_s = \pi/\sqrt{2b}$. It follows that $(n_1 n_{e0})^{1/2}\tau_s = (k_{12}\beta_{2e})^{-1/2} = $ const for a fixed value of E/n_1. For large E/n_1 we have $A \to 0$, and $\tau_s \to 2/(n_{e0}\beta_{2e} + n_1\beta_{1e} - \nu_{Da})$ is only weakly dependent on n_{e0}.

Figure 3a also gives experimental values of the parameter $(n_1 n_{e0})^{1/2}\tau_s$, which for $E/n_1 = $ const remains constant to within the experimental error for n_{e0}, n_1, and τ_s varying over wide limits. For large E/n_1 [Fig. 3b, Fig. 4b] τ_s becomes almost independent of n_{e0}, as predicted by our theory.

We also note that the function $n_e(t)$ calculated using (8)–(9) accurately describes the experimentally observed increase in the current and plasma emission. We thus conclude that theory and experiment are in both qualitative and quantitative agreement.

The above equations can be used to analyze the time change of the radial distribution $n_e(r, t)$ when an electric field is suddenly applied to a gas for which the initial distributions $n_{e0}(r)$ and $n_{20}(r)$ are known. This problem is of interest in terms of understanding the mechanism responsible for formation and constriction of the current channel in a pulsed discharge.[17]

The solutions of system (5), (6) show how the initial distribution $n_{e0}(r)$ is deformed when a field is switched on. In the situation discussed above (corresponding to $A > 0$) Eqs. (8)–(9) imply that the growth rate of $n_e(t)$ depends strongly on n_{e0}, particularly for large values of A ($A \simeq 2/b$). This results in a sudden increase in the magnitude of the initial irregularities in $n_e(r)$ for $t < \tau_s$. As an illustration, Fig. 5 shows curves giving the time dependence of $n_e(r)$ calculated from (9b) for $E/n_1 = 12$ Td and $n_{e0} = 10^{10}$ cm^{-3} for an argon discharge. According to Ref. 9, the initial n_{e0} and n_{20} distributions in a glow discharge at moderate pressures can be approximated by Bessel functions, and we took $M_0 = 0.1$. Under these assumptions, we see that the theory predicts that the distributions will become highly nonuniform at times $t \gtrsim \tau_s$ after the field is turned on.

For large E/n_1, $A < 0$ and the growth of n_e during the slow stage [cf. (9a)] is determined by direct ionization.

The form of the radial distribution $n_e(r)$ will then be similar to the initial distribution and no well-defined plasma column is produced. Our model thus predicts slight deformation of the initial distribution $n_{e0}(r)$ for $A < 0$ but substantial deformation when $A > 0$.

Experiments (cf. Refs. 18, 19) have shown that ionization occurs uniformly over a cross section of the discharge tube when a field is applied to a preionized gas; however, if $p > p_0$ the ionization is highly nonuniform and a narrow plasma column forms on the axis. In particular, for argon $p_0 = 1$ torr for $R = 2$-4 cm (R is the tube radius) [Ref. 18] and $p_0 = 2$-3 torr for $R = 1$ cm [Ref. 19]. For discharge in helium, the experiments indicate that ionization is uniform for pressures $\lesssim 10$ torr when $R = 1$ cm.

Our model accounts well for these experimental findings. Figure 6 shows calculated curves for a discharge in argon. We see that for $pR < 1$ cm·torr, n_e cannot increase unless $A < 0$. In this case ionization develops more uniformly in the bulk, in good agreement with experiment. Since for the heavy inert gases (Ne, Ar, Kr, Xe), k_{12}, β_{1e}, β_{2e}, ν_{Da} all have the same order of magnitude, the corresponding curves behave similarly for similar values of pR. Helium is an exception, since under our conditions ν_{Da} is much larger and β_{1e} much smaller than for the heavy inert gases. The region $A < 0$ will therefore correspond to larger products pR, and this is also in agreement with the experimental findings.

We have thus developed a model for the initial stage of ionization relaxation in a pulsed inert-gas discharge plasma at moderate pressures for E/n_1 values corresponding to equilibrium ionizations $n_e^0/n_1^0 \gg 10^{-4}$. We conclude from a comparison of the experimental spatial and time dependences of n_e that the model is quite accurate. We have shown that the increase of n_e with time is explosive because atoms accumulate in the lowest excited states. Our results are important for analyzing the role of stepwise ionization processes in the buildup of instabilities in self-sustained and externally maintained discharges.[17,20] Under our conditions, the above equations have the advantage that they clearly exhibit the various ionization mechanisms, so that their specific effects can be studied as a function of the experimental conditions. Since the effects studied in this work are characteristic of ionization whenever a field is suddenly applied to a weakly ionized gas, they must be allowed for when studying emission mechanisms in pulsed gas lasers, gas breakdown, laser sparks, etc.

[1]A. V. Eletskii, Usp. Fiz. Nauk 125, 279 (1978) [Sov. Phys. Usp. 21, 502 (1978)].

[2]G. V. Naidis, Zh. Tekh. Fiz. 47, 941 (1977) [Sov. Phys. Tech. Phys. 22, 562 (1977)].

[3]A. A. Belevtsev, Teplofiz. Vys. Temp. 17, 1138 (1979).

[4]L. M. Biberman, V. S. Vorob'ev, and I. T. Yakubov, Usp. Fiz. Nauk 107, 353 (1972); 128, 233 (1979) [Sov. Phys. Usp. 15, 375 (1973); 22, 411 (1979)].

[5]N. L. Aleksandrov, A. M. Konchakov, and É. E. Son, Zh. Tekh. Fiz. 50, 481 (1980) [Sov. Phys. Tech. Phys. 25, 291 (1980)].

[6]W. L. Nighan, Appl. Phys. Lett. 32, 424 (1978).

[7]B. M. Smirnov, Ions and Excited Atoms in Plasmas [in Russian], Atomizdat, Moscow (1974).

[8]M. G. Voitik, A. G. Molchanov, and Yu. G. Popov, Kvantovaya Elektron. (Moscow) 4, 1722 (1977) [Sov. J. Quantum Electron. 7, 976 (1977)].

A. A. Kudryavtsev and V. N. Skrebov   34

DOCKET ALARM

Explore Litigation Insights

Docket Alarm provides insights to develop a more informed litigation strategy and the peace of mind of knowing you're on top of things.

Real-Time Litigation Alerts

Keep your litigation team up-to-date with **real-time alerts** and advanced team management tools built for the enterprise, all while greatly reducing PACER spend.

Our comprehensive service means we can handle Federal, State, and Administrative courts across the country.

Advanced Docket Research

With over 230 million records, Docket Alarm's cloud-native docket research platform finds what other services can't. Coverage includes Federal, State, plus PTAB, TTAB, ITC and NLRB decisions, all in one place.

Identify arguments that have been successful in the past with full text, pinpoint searching. Link to case law cited within any court document via Fastcase.

Analytics At Your Fingertips

Learn what happened the last time a particular judge, opposing counsel or company faced cases similar to yours.

Advanced out-of-the-box PTAB and TTAB analytics are always at your fingertips.

API

Docket Alarm offers a powerful API (application programming interface) to developers that want to integrate case filings into their apps.

LAW FIRMS
Build custom dashboards for your attorneys and clients with live data direct from the court.

Automate many repetitive legal tasks like conflict checks, document management, and marketing.

FINANCIAL INSTITUTIONS
Litigation and bankruptcy checks for companies and debtors.

E-DISCOVERY AND LEGAL VENDORS
Sync your system to PACER to automate legal marketing.

fastcase®
Smarter legal research.